Nonlinear Talbot Effect

Yong Zhang,[1,2,3] Jianming Wen,[1,2] S. N. Zhu,[1] and Min Xiao[1,2,3,*]

[1]National Laboratory of Solid State Microstructures and Department of Physics, Nanjing University, Nanjing 210093, China
[2]Department of Physics, University of Arkansas, Fayetteville, Arkansas 72701, USA
[3]School of Modern Engineering and Applied Science, Nanjing University, Nanjing 210093, China

(Received 20 January 2010; published 7 May 2010)

We propose and experimentally demonstrate the nonlinear Talbot effect from nonlinear photonic crystals. The nonlinear Talbot effect results from self-imaging of the generated periodic intensity pattern at the output surface of the crystal. To illustrate the effect, we experimentally observed second-harmonic Talbot self-imaging from 1D and 2D periodically poled $LiTaO_3$ crystals. Both integer and fractional nonlinear Talbot effects were investigated. The observation not only conceptually extends the conventional Talbot effect, but also opens the door for a variety of new applications in imaging technologies.

DOI: 10.1103/PhysRevLett.104.183901 PACS numbers: 42.30.Kq, 42.65.Ky, 42.70.Mp

The Talbot effect [1,2], a near-field diffraction phenomenon in which self-imaging of a grating or other periodic structure replicates at certain imaging planes, holds a variety of applications in imaging processing and synthesis, photolithography, optical testing, optical metrology, spectrometry, optical computing [3], as well as in electron optics and microscopy [4]. Recent progress has been made in areas such as atomic waves [5,6], nonclassical light [7], waveguide arrays [8], and x-ray phase imaging [9]. However, all the above achievements are limited in studying properties of input fundamental signals. In this Letter, we demonstrate, for the first time, the nonlinear Talbot effect, i.e., the formation of second-harmonic (SH) self-imaging instead of the fundamental one from periodically poled $LiTaO_3$ (PPLT) crystals. This demonstration not only maintains all characteristics of the conventional Talbot effect, but offers a new way to image objects with periodic structures with higher spatial resolution. The conceptual extension achieved here thus opens a door for broader scopes of applications in imaging techniques.

The conventional Talbot effect is well understood by the Fresnel-Kirchhoff diffraction theory, as first explained analytically by Lord Rayleigh in 1881 [2], attributing its origin to the interference of diffracted beams. The simplicity and beauty of such Talbot self-imaging have since then attracted many researchers and resulted in numerous interesting and original applications that represent competitive solutions to various scientific and technological problems. The optical self-imaging phenomenon usually requires a highly spatially coherent illumination. The self-imaging disappears when the lateral dimensions of the light source are increased. As noted a long time ago, when the source is made spatially periodic and it is placed at the proper distance in front of a periodic structure, a fringe pattern is formed in the space behind the structure. The first example of this type was performed by Lau [10], who used two amplitude gratings of the same spatial period illuminated incoherently. However, up to today, all the research on the self-imaging has been limited in studying the properties of the input beams and using *real* gratings for imaging. Bypassing these limitations will not only enrich the conventional self-imaging research, but also offer new methods for imaging technologies. Here, we present the first experimental demonstration beyond the conventional Talbot effect, in which the observed self-images are not produced by the input fundamental beam but by the SH field generated in PPLT nonlinear crystals. In our experiment, the *grating* is the periodic intensity patterns appearing on the output surface of the crystal due to the periodic domain structures, i.e., the modulated second-order nonlinear susceptibility. This difference thus distinguishes our results from the conventional self-imaging research.

PPLT crystals have been extensively used as a workhorse for laser frequency conversion [11], optical switching [12], wave-front engineering [13], and quantum information processing [14]. Numerous interesting phenomena have been discovered in both 1D and 2D nonlinear photonic crystals, such as solitons [15], entangled photons [16], conical second-harmonic generation (SHG) [17,18], and nonlinear Čerenkov radiation [19]. Benefitting from their modified nonlinear properties, here we report a novel SH Talbot self-imaging demonstrated with the use of such crystals. Different from the conventional Talbot effect [1,3], the observed self-imaging is a consequence of the $\chi^{(2)}$ nonlinear optical process, which we call the nonlinear Talbot effect. As mentioned before, the Talbot effect is attributed to the interference of diffracted beams from periodic structures, a prerequisite condition to realize such an effect [1–3]. In PPLT crystals, this condition is fulfilled by the periodic patterns of the SH intensity difference distributed on the output surface. The SH intensity generated from the domain walls is different from that inside domains because the nonlinear coefficients near the nonideal domain walls will be changed due to the

crystal lattice distortion after the poling process [20]. In the experiment, we have directly observed periodically distributed SH intensity patterns in recorded self-images. Although the observed phenomenon well resembles the conventional Talbot effect, several interesting features distinguish this demonstration from the previous observations. Besides no real grating used in the experiment, spatial resolution improvement by a factor of 2, due to frequency doubling, is powerful to high-resolution imaging, compared with the simple input-pump imaging. In principle, if the material allows the Nth-order harmonic generation, spatial resolving power can be enhanced by N times using the nonlinear Talbot effect reported here. Moreover, this experiment conceptually extends the conventional Talbot effect and thus paves a way for new applications.

The 1D and 2D PPLT slices were fabricated through an electric-field poling technique at room temperature [21]. In the experiments, we used a femtosecond mode-locked Ti:sapphire laser operating at a wavelength of 800 nm as the fundamental input field. The pulse width is ~100 fs with a repetition rate of 82 MHz. As shown in Fig. 1, the fundamental beam from the Ti:sapphire laser was first reshaped by a telescope device, composed of two focusing lenses, to achieve a near-parallel beam with a spot size of ~100 μm, which propagates along the z axis of the PPLT sample and whose polarization is parallel to the x axis of the crystal. Although $LiTaO_3$ crystal has a space group of $3m(C_{3v})$, only the d_{21} component contributes to the SHG process in our experimental configuration [22]. After the sample, a bandpass filter was used to filter out the near-infrared fundamental field. The generated SH intensity pattern was magnified by an objective lens and projected onto a CCD camera. The SH patterns at different imaging planes were recorded by moving the objective lens along the SH propagation direction, which was controlled by a precision translation stage. We emphasize that the nonlinear Talbot effect is a lensless imaging process. The objective used here is to magnify the self-images for easy observations.

Figs. 2 and 3, respectively, show the integer SH self-images from 1D and 2D PPLT crystals. In the experiment, we have sequentially recorded such integer Talbot self-images at about several Talbot lengths. For simplicity, we arranged d_{21} as the only nonzero nonlinear coefficient in the tensor to contribute to the collinear SHG process. To verify this, we measured the polarization of the generated SH wave and found that its polarization was indeed along the y axis of the crystal. As described above, d_{21} at the domain walls is different from that inside the domains. Such periodic domain structures result in the generated SH intensity patterns displaying the same periodicity at the sample output surface. An *imaginary* grating is thus formed for self-imaging. From the Fresnel-Kirchhoff diffraction theory, the diffracted field amplitude $A(\vec{r}_1)$ is defined in terms of the aperture function of the object $t(\vec{r})$ and the coherent amplitude of the source $S(\vec{r}_s)$. Here $\vec{r}_1$, $\vec{r}$, and $\vec{r}_s$ are located at the observation, object, and source planes, respectively. The diffracted amplitude $A(\vec{r}_1)$ is given by

$$A(\vec{r}_1) = \frac{\exp[2i\pi(d_1 + d_2)/\lambda]}{i\lambda d_1 d_2} \int d\vec{r}_s S(\vec{r}_s) \int d\vec{r} t(\vec{r}) \times \exp\left[\frac{i\pi|\vec{r} - \vec{r}_s|^2}{\lambda d_1}\right] \exp\left[\frac{i\pi|\vec{r}_1 - \vec{r}|^2}{\lambda d_2}\right], \quad (1)$$

where d_1 is the propagation distance between the object and the source, and d_2 is the distance from the object to the observation plane. In our experiment, the SH source may be treated as a plane wave or a Gaussian beam. The aperture function comes from the spatially periodic domain structures, i.e., the periodically engineered $\chi^{(2)}$. One notable difference from conventional self-imaging is that λ in Eq. (1) is the SH wavelength, which is half of the wavelength λ_p of the fundamental input beam. This difference leads to a factor of 2 in imaging resolution improvement, compared with the traditional direct input-output measurement.

In our first experiment, a 1D PPLT sample with a domain period of $a = 8.0$ μm and a duty cycle of ~50% [see the SEM picture shown in Fig. 2(a)] was chosen to illustrate the effect. Figs. 2(b) and 2(c) are the recorded self-images on the first and third Talbot planes, respectively. For a plane-wave illumination, the self-images repeat at multiples of the SH Talbot length $z_T = 4a^2/\lambda_p$, which gives 320 μm and 960 μm for the first and third Talbot imaging planes. The experimentally measured lengths were 330 μm ± 5 μm and 1020 μm ± 10 μm, respectively.

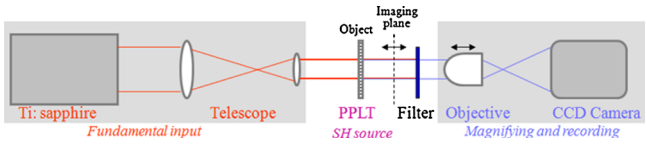

FIG. 1 (color online). Experimental setup. The PPLT sample is placed at the waist plane of the fundamental wave. The patterns on different imaging planes are recorded by a CCD camera through moving the objective.

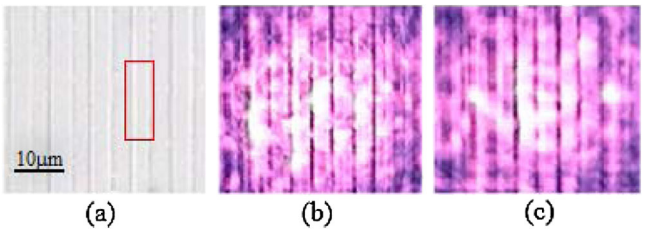

FIG. 2 (color online). 1D SH Talbot self-imaging. (a) The domain structure of the 1D PPLT crystal; (b) the SH self-image at the first Talbot plane; (c) the SH self-images at the third Talbot plane. The marked domain in (a) is a little narrower than the others.

The discrepancy between the experiment and theory can be readily corrected by taking into account the Gaussian profile of the beam, which reinterprets the SH Talbot length as $z_T = 4(a^2/\lambda_p)(r_z/r_0)^2$, where r_z and r_0 represent the Gaussian beam radii at the imaging plane and the waist plane. In the experiments, the PPLT sample was placed at the waist plane of the Gaussian beam. The corrected theoretical lengths are now 320 μm with $r_z/r_0 = 1.00$ and 1018 μm with $r_z/r_0 = 1.03$, consistent with the experimental data. Periodic SH interference fringes are clearly observable on the first Talbot plane [Fig. 2(b)] and the period coincides with the periodicity of the domain structure. The bright fringes correspond to the domains exactly. The intensities from positive or negative domains have no appreciable difference because the value of the nonlinear coefficient inside the domains does not change during the poling process. The dark fringes correspond to the domain walls. In the self-imaging, the SH intensity produced at the domain walls is much weaker than that inside the domains. From Fig. 2(b), the width of the domain walls is estimated to be 0.5 μm, which agrees with the reported range from 100 nm to few microns [23]. One difference between the SEM image [Fig. 2(a)] and the self-image [Fig. 2(b)] is that the SEM imaging is sensitive to the imperfections in the domain structure (the marked square) while the self-imaging produces a uniform interference pattern. It is because only the periodically distributed SH light is self-imaged at the Talbot planes while the nonperiodic part is not reproduced. This could be useful for the application of optical lithography. We also experimentally found that the image qualities after the third Talbot plane became worse than those at the first and second planes. One reason is that higher-order diffraction fields cannot be totally collected by the CCD camera with a limited numerical aperture.

To illustrate the integer SH Talbot effect from a 2D modulated nonlinear crystal, a hexagonally-poled $LiTaO_3$ slice, was adopted in the second experiment. The period of the domain structure of the sample is $a = 9.0$ μm and the duty cycle is $\sim$30% as shown in the SEM image in Fig. 3(a). The SH self-images were also successively observed at several Talbot imaging planes. For the ideal plane-wave illumination, the Talbot length is deduced to be $z_T = 3a^2/\lambda_p$. Taking into account the Gaussian profile, the SH Talbot length is corrected to be $z_T = 3(a^2/\lambda_p) \times (r_z/r_0)^2$. Figs. 3(b) and 3(c) show the images recorded at the first and third SH Talbot planes, respectively. Same as for the 1D case, the SH waves generated at the domain walls are weaker than that created inside the domains. The domain wall in the 2D structure exhibits a ring-shaped structure [Fig. 3(b)], while it appears as a dark line in the 1D PPLT [Fig. 2(b)]. Similar as the 1D structure, the qualities of the self-images after the third Talbot plane [Fig. 3(c)] become worse due to the loss of higher-order SH diffractions. The measured first and third SH Talbot lengths were 315 μm $\pm$ 5 μm and 970 μm $\pm$ 10 μm,

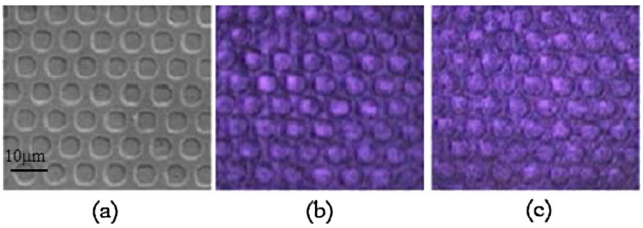

FIG. 3 (color online). 2D SH Talbot self-imaging. (a) The domain structure of the hexagonally poled $LiTaO_3$ crystal; (b) the SH self-image at the first Talbot plane; (c) the SH self-images at the third Talbot plane.

which agree well with the calculated 304 μm ($r_z/r_0 = 1.00$) and 966 μm ($r_z/r_0 = 1.03$), respectively.

Besides these integer SH Talbot effect, in the third experiment we have also investigated the fractional SH self-images occurring at the intermediate Talbot distances, $z = (p/q)z_T$, where p and q are integers with no common factor. It is well known that fractional Talbot effect [24–26] has a close connection with fractional revivals, quantum carpet [27], and Gauss sums [28]. Compared with the integer self-imaging, fractional SH Talbot effect exhibits more interesting and complicated interference patterns. We have experimentally observed such patterns for both 1D and 2D PPLT crystals. In the 1D case, because of the limited illumination area on the sample, the quality of fractional self-images is greatly reduced and becomes blurry in contrast with the integer cases [Figs. 2(b) and 2(c)]. The situation is dramatically changed for the 2D case, where the SH factional Talbot images have high quality and show number of unique properties in comparison with the integer case. In Figs. 4(a)–4(f), we present several representative fractional self-images with different fractional (p/q) parameters. For instance, the SH interference pattern at the $z_T/7$ plane [Fig. 4(a)] is periodically distributed bright spots with the same lattice structure as in the integer case. In Figs. 4(b) and 4(c), the period of the hexagonal structure is halved. In Figs. 4(c)–4(f), a 30° rotation of the

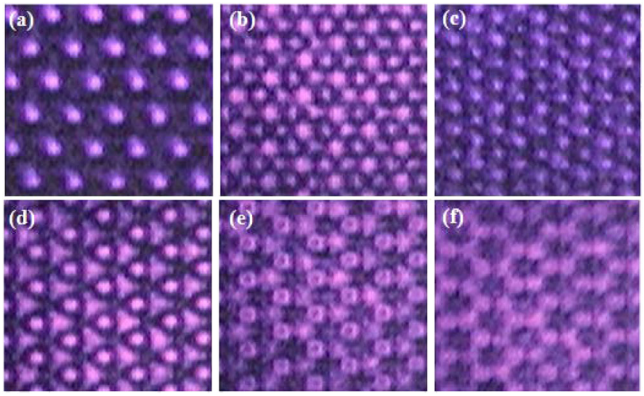

FIG. 4 (color online). The SH patterns (a)–(f) are corresponding to fractional Talbot images at different fractional Talbot planes.

structure is obviously observable and even a π-phase shift can be deduced from Figs. 4(d)–4(f). We found that the fractional Talbot images are very sensitive to the precision positions of the imaging planes. Further detailed studies of these fractional SH Talbot effects will be presented elsewhere.

In recent years, SH imaging technique has been developed into a powerful near-field imaging tool for visualizing various ferroic domains [29], carrier motion [30], biomolecular array [31], and collagen modulation [32]. Comparing with the conventional SH imaging, such SH Talbot self-imaging does not need an imaging lens and no reference SH wave is needed, which greatly simplifies the experimental setup. For periodically-poled ferroelectric domains, although chemical etching method is adopted as a standard procedure to look at the domain structures [33], one major disadvantage of this method is that the sample surface is damaged. The newly observed nonlinear Talbot effect provides a better (optical) way to easily check the domains without damaging the sample surfaces. This will be very helpful for inspecting integrated nonlinear optical devices such as nonlinear photonic waveguides and wavelength conversion devices, which cannot be done by the conventional Talbot effect. More importantly, the conceptual generalization demonstrated here is not limited to the optical signals, and could also apply to other research fields where similar situations may exist. This effect can also be further considered with nonclassical light states [7] to achieve sub-Rayleigh images. Generally speaking, the demonstrated effect not only enriches conventional imaging techniques, but also offers a new method for imaging in broad applications.

We acknowledge partial support from the National Science Foundation (U.S.A.) and partial support by the 111 Project B07026 (China).

*mxiao@uark.edu

[1] H. F. Talbot, Philos. Mag. **9**, 401 (1836).
[2] L. Rayleigh, Philos. Mag. **11**, 196 (1881).
[3] K. Patorski, Prog. Opt. **27**, 1 (1989).
[4] J. M. Cowley, *Diffraction Physics* (North-Holland, Amsterdam, 1995).
[5] M. S. Chapman *et al.*, Phys. Rev. A **51**, R14 (1995).
[6] C. Ryu *et al.*, Phys. Rev. Lett. **96**, 160403 (2006).
[7] K.-H. Luo *et al.*, Phys. Rev. A **80**, 043820 (2009).
[8] R. Iwanow *et al.*, Phys. Rev. Lett. **95**, 053902 (2005).
[9] F. Pfeiffer *et al.*, Nature Mater. **7**, 134 (2008).
[10] E. Lau, Ann. Phys. (Leipzig) **437**, 417 (1948).
[11] S. N. Zhu, Y. Y. Zhu, and N. B. Ming, Science **278**, 843 (1997).
[12] C. Langrock *et al.*, J. Lightwave Technol. **24**, 2579 (2006).
[13] Y. Q. Qin *et al.*, Phys. Rev. Lett. **100**, 063902 (2008).
[14] P. Kumar *et al.*, Quant. Info. Proc. **3**, 215 (2004).
[15] H. Kim *et al.*, Opt. Lett. **28**, 640 (2003).
[16] X. Q. Yu *et al.*, Phys. Rev. Lett. **101**, 233601 (2008).
[17] P. Xu *et al.*, Phys. Rev. Lett. **93**, 133904 (2004).
[18] S. M. Saltiel *et al.*, Phys. Rev. Lett. **100**, 103902 (2008).
[19] Y. Zhang *et al.*, Phys. Rev. Lett. **100**, 163904 (2008).
[20] M. Bazzan *et al.*, in *Ferroelectric Crystals for Photonic Applications*, edited by P. Ferraro, S. Grilli, and P. De Natale, (Springer-Verlag, Berlin, Heidelberg, 2009).
[21] S. N. Zhu *et al.*, J. Appl. Phys. **77**, 5481 (1995).
[22] R. W. Boyd, *Nonlinear Optics* (Academic, New York, 2003), 2nd ed.
[23] T. J. Yang *et al.*, Phys. Rev. Lett. **82**, 4106 (1999).
[24] J. T. Winthrop and C. R. Worthington, J. Opt. Soc. Am. **55**, 373 (1965).
[25] M. Paturzo *et al.*, Opt. Lett. **31**, 3164 (2006).
[26] C.-S. Guo *et al.*, Opt. Lett. **32**, 2079 (2007).
[27] M. V. Berry, I. Marzoli, and W. P. Schleich, Phys. World **14**, 39 (2001).
[28] D. Bigourd *et al.*, Phys. Rev. Lett. **100**, 030202 (2008).
[29] M. Fiebig *et al.*, Nature (London) **419**, 818 (2002).
[30] T. Manaka *et al.*, Nat. Photon. **1**, 581 (2007).
[31] P. J. Campagnola and L. M. Loew, Nat. Biotechnol. **21**, 1356 (2003).
[32] E. Brown *et al.*, Nature Med. **9**, 796 (2003).
[33] V. Bermudez *et al.*, J. Cryst. Growth **191**, 589 (1998).